18TH WORLD CONFERENCE ON EARTHQUAKE ENGINEERING
WCEE2024
MILAN

MILAN, ITALY
30TH JUNE - 5TH JULY 2024

www.wcee2024.it

COMPARISON BETWEEN GROUND MOTION DATA AND SEMI-EMPIRICAL SPECTRAL GROUND MOTION PREDICTION EQUATIONS FOR GEOTHERMAL-INDUCED MICRO-EARTHQUAKES

F. Taddei[1], S. Keil[2], A. Kumawat[1] & G. Müller[1]

[1] Technical University of Munich, TUM School of Engineering and Design, Chair of Structural Mechanics, Munich, Germany, francesca.taddei@tum.de, aditi.kumawat@tum.de, gerhard.mueller@tum.de

[2] Ludwig-Maximilians-Universität München, Department of Earth and Environmental Sciences, Munich, Germany, s.keil@lmu.de

Abstract: *Geothermal energy plays a substantial role in Germany's energy production, particularly in Bavaria. Yet, it carries the risk of induced seismicity, which concerns regions with geothermal plants close to urban areas. Seismic hazard assessment in these areas faces challenges due to limited ground motion observations. To address this, it is possible to develop Ground Motion Prediction Equations (GMPEs) for geothermal-induced (GI) earthquakes. Compared to tectonic events, GI-earthquakes have unique characteristics, such as shallow depths and small magnitudes, which make them challenging to model. Our study focuses on characterizing ground motions for micro-earthquakes in Southern Germany. We conduct a statistical analysis of recorded seismic data in the Greater Munich Area, combining this data with physics-based simulations. We compare this hybrid dataset with an established GMPE model for GI-events. The simulated data fall within the variability of the recorded data, for periods above 0.1 s. However, at shorter periods, the cutoff frequency imposed in the simulations leads to significant differences, especially for vertical spectral velocities. Discrepancies between the observations and the selected GMPEs, especially at short periods, could be attributed to the challenges in estimating moment magnitudes for small earthquakes.*

1 Introduction

Geothermal energy is rising in Germany, constituting a significant portion of the nation's energy production and playing an even more substantial role in Bavaria's energy supply. However, it comes with induced seismicity risks, particularly in regions with geothermal power plants near urban areas. While the risk due to geothermal-induced (GI) seismicity is generally low, certain regions in Southern Germany may be affected due to their low tectonic activity (Grünthal 2014).

Seismic hazard and risk analysis face challenges, particularly in regions with limited ground motion observations. To adapt, researchers often modify ground motion models (GMMs) initially designed for active areas to suit specific seismological conditions, using simulations calibrated with recorded data or alternative sources (Bommer et al. 2016). To reduce uncertainty, novel concepts suggest employing a core model (backbone) and applying scaling factors for regional variations aided by a logic tree process (Edwards et al. 2013). Bayesian and frequentist approaches can be used to select and weight relevant models (Baker et al. 2016). Ground Motion Prediction Equations (GMPEs) are a subset of the GMMs and estimate ground motion characteristics (such as the peak ground acceleration and spectral quantities) for seismic hazard assessments.

GMPEs consider various parameters like earthquake magnitude, epicentral or hypocentral distance, site conditions, focal depth, rupture mechanism, and source-to-site azimuth. Existing GMPEs designed for tectonic earthquakes may not reliably extrapolate to induced earthquakes. The shallow focal depths of induced

earthquakes make them particularly influenced by the heterogeneous properties of the upper crust, leading to significant variability in ground motion characteristics. On the other hand, well-known uppermost crustal conditions and the availability of data from instrumented geothermal power plants (GPPs) provide opportunities to develop tailored GMPEs and decrease uncertainties related to specific applications.

Several studies have focused on GMPEs for induced earthquakes, including one that proposed a basis of 36 models derived from stochastic simulations and highlights the importance of incorporating several models due to high epistemic uncertainty in seismic hazard assessments (Douglas et al. 2013). Another study analysed a global database of geothermal power plant-induced earthquakes and developed various ground motion models for risk assessment and mitigation (Khansefid et al. 2022). Site-specific GMPEs for probabilistic seismic hazard analysis (PSHA) for Southern Germany were proposed for Unterhaching, Landau, and Insheim, emphasizing the significance of spectral characteristics in ground motion analysis (Sisi et al. 2017). Some studies introduced innovative approaches for ground motion estimation, such as generating comprehensive ground motion maps using machine learning and assessing uncertainties in peak ground velocity values (Steinberg et al. 2023).

This contribution is concerned with the characterization of the ground motions and spectral quantities for GPP-induced micro-earthquakes in Southern Germany. We begin with a statistical analysis of available recorded seismic datasets for GPPs in the Greater Munich Area. We then merge the scarce dataset from Munich with physics-based simulation data. Finally, we compare the hybrid data set with a selected existing set of GMPEs.

2 Geothermal areas and GPPs

The Molasse basin (Figure 1), spanning a large area north of the Alps, features Tertiary sediments overlying Mesozoic limestone layers and the Variscan crystalline basement. The Poing geothermal project within this basin includes two wells, Th1 and Th2, with circulation starting in 2012 and seismic activity observed in late 2016 (Keil et al. 2022). The Unterhaching geothermal power plant has an electrical capacity of around 3.36 megawatts and a thermal capacity of up to 70 megawatts. It began operations in 2007, utilizing the Kalina process for electricity generation, with seismicity starting in 2008. The Kalina plant was later decommissioned in 2017 due to shifting priorities toward district heating for more households (Wolfgramm et al. 2007). Table 1 gives the key data of the considered geothermal power plans.

3 Data

GMPEs can be developed by analysing recorded and simulated seismic ground motions. Recorded ground motions, derived from past earthquake events, provide invaluable data for calibration and validation. Simulated ground motions, on the other hand, offer insights into potential scenarios that may not have been observed in recorded data. The synergy between recorded and simulated seismic ground motions is essential in enhancing the accuracy and reliability of GMPEs, ultimately contributing to more effective earthquake risk mitigation and preparedness strategies. Here we present the recorded data for Poing (POI) and Unterhaching (UH) in the Greater Munich Area and we compare them with data from a third location outside Bavaria, Insheim (INS) (Taddei et al. 2022). Moreover, we extend the comparison including simulation data for a hypothetical GPP in the centre of the city of Munich and varying seismological parameters within a realistic range. The parameter variation was decided based on the evaluation of larger recorded data set from the third location Insheim, performed in previous studies (Taddei et al. 2022).

The recorded and simulated data were made available by the Department of Earth and Environmental Sciences of the LMU. Most induced seismic events in our analysis were initially provided with their local magnitude, denoted as $\mathrm{M_L}$. To convert these values to moment magnitude ($\mathrm{M_w}$), we employed the relations for calculating $\mathrm{M_w}$ for Central and Northern Europe (Grünthal et al. 2009).

$$\mathrm{M_w} = 0.67\ (\pm 0.11) + 0.56(\pm 0.08)\mathrm{M_L} + 0.046(\pm 0.013)\mathrm{M_L^2} \quad (1)$$

It must be pointed out that scaling $\mathrm{M_w}$ from $\mathrm{M_L}$ introduces additional uncertainties in the derivation of the GMPE, especially at low magnitudes (Edwards et al. 2010).

3.1 Recorded data for Poing and Unterhaching

Table 2 lists the considered earthquakes with M_w ranging from 1.83 to 2.05. Figure 2 shows the locations of the considered seismic stations and GPPs. Table 5 in the annex gives the event-station matrix. The data

acquisition was carried out at a minimum sample rate of 250 Hz. The soil class can be considered stiff soil (EC8 - C), being V_s, the mean shear velocity within the first 30 m of depth, ~350 m/s. Further details about the events and the focal mechanisms can be found in (Keil et al. 2022). Table 3 summarizes the Parameter ranges of the recorded earthquakes in Insheim.

To ensure the quality and reliability of the raw data, we conducted a series of enhancements, including wavelet denoising, baseline adjustment, and high-pass filtering, as outlined in previous studies (Khansefid et al. 2022). This approach has been effectively employed in the past to improve seismic recordings characterized by low amplitudes during GI-events and weak signals in the Iranian plateau (Khansefid et al. 2019). Figure 3 compares raw and denoised signals for two randomly chosen events and stations, showing that the filtering process does not alter the amplitudes of the signals.

3.2 Simulation data for Munich

The seismic wave simulations for a hypothetical GPP in the city centre of Munich (MUC) are conducted with the SALVUS spectral element code (Afanasiev et al. 2019), a versatile software designed for full waveform modeling in both 2D and 3D. SALVUS provides tools for efficient mesh generation, including complex media and topography. The model's applicability was verified in previous studies for Poing, where the 3D subsurface model, the parameter uncertainties, and the shake maps were investigated (Keil et al. 2022).

For the simulations, due to the high computational costs, the element size was chosen such that at least frequencies up to 10 Hz were considered. A polynomial degree of 1 and a minimum of 1.5 elements per wavelength are employed, with adaptive meshing reducing the number of elements and grid points in the mesh. For minor earthquakes, we assume the fault behaves as a point source with instantaneous rupture. In this scenario, the source time function is represented by a delta pulse, which is approximated using a sinc-function with a uniform power spectrum up to 10 Hz. Subsequently, the simulated waveforms are subjected to bandpass filtering between 1 and 10 Hz. The limited frequency range represents an assumption that must be verified and adapted if necessary.

Table 4 gives a summary of the seismological features of the simulated earthquakes. Figure 9, in the annex, gives the distribution of the simulation stations. The subsurface can be considered very similar to the other locations in the Greater Munich area, and therefore, the site conditions at different locations do not play a major role in the variability of the ground motions.

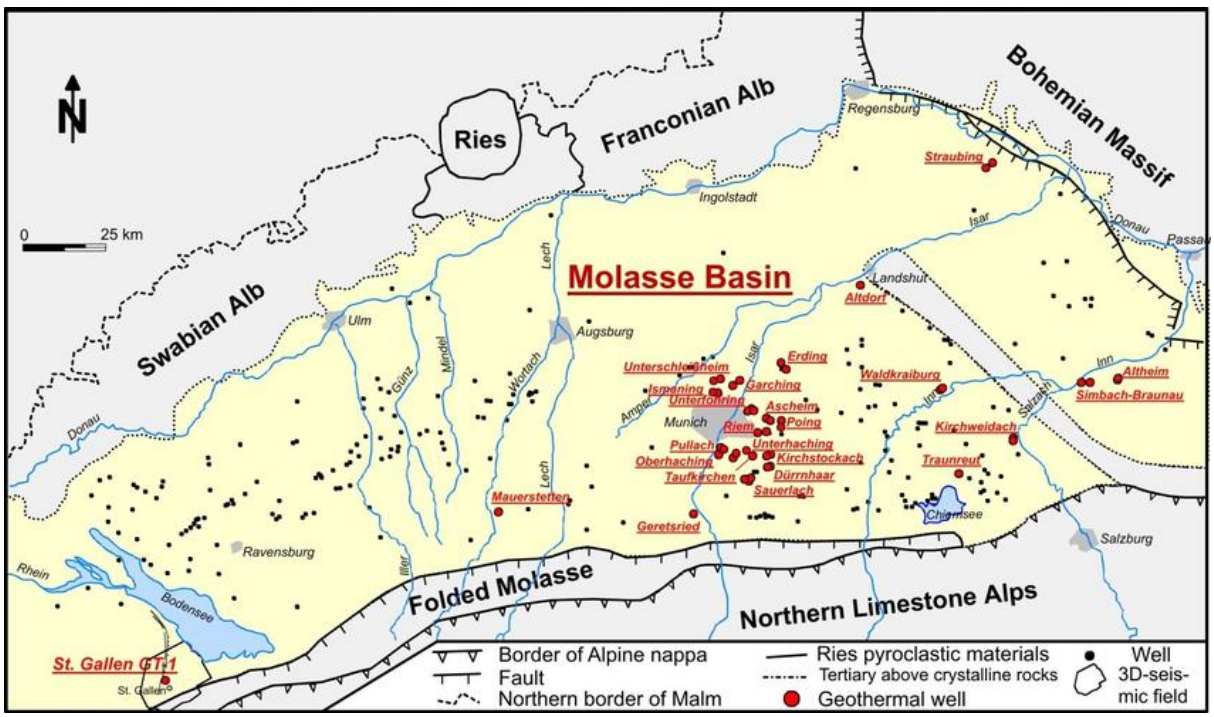

Figure 1. Distribution of geothermal wells in the Molasse basin (red), mostly used for power generation, after (Beichel et al. 2014).

Table 1. Key data of the considered geothermal power plans.

GPP	**Start time**	**LAT** (°)	**LON** (°)	**Max. well depth** (km)
Poing	2016	48.19	11.79	3
Unterhaching	2007	48.06	11.60	3.6

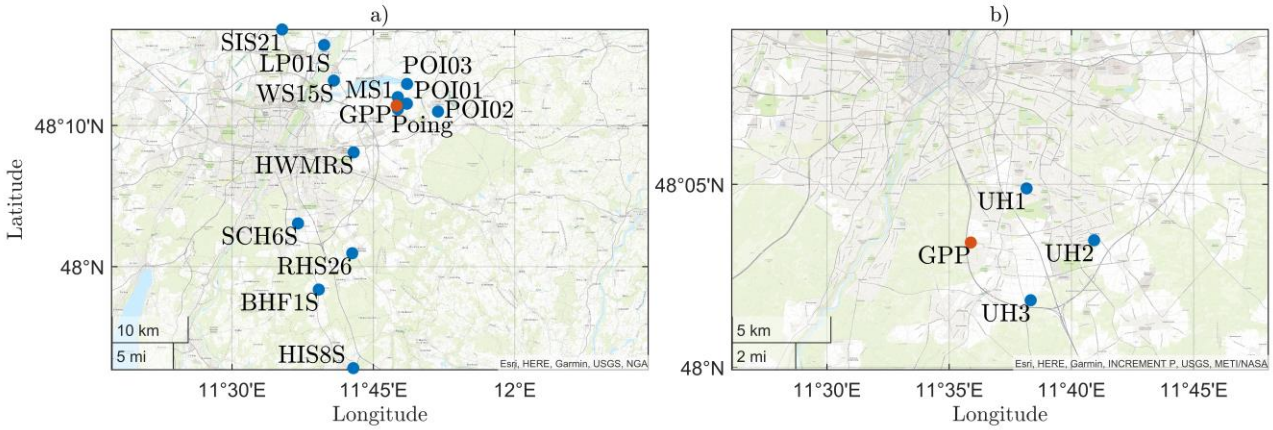

Figure 2. Distribution of the considered stations and the GPPs for a) Poing and b) Unterhaching. The locations of the GPP do not coincide with the epicenters.

Table 2 Description of the recorded earthquakes in Poing and Unterhaching considered in this study.

Event		**Date** (dd-mm-yyyy)	**Time** (hh:mm:ss)	**LON** (°)	**LAT** (°)	**Depth** (km)	M_L	M_w	**Recording stations** (E,N,V each)
1	Unterhaching (UH)	16-Apr-2013	21:51:42	48.05	11.64	4.7	2.1	2.05	3
2		16-Apr-2013	21:51:48	48.05	11.64	4.7	2.1	2.05	3
3	Poing (POI)	19-Nov-2016	17:41:05	48.19	11.79	3.9	1.2	1.41	2
4		27-Nov-2016	14:52:21	48.19	11.79	5.0	1.0	1.28	1
5		07-Dec-2016	05:28:54	48.19	11.79	6.0	2.1	2.05	4
6		10-Dec-2016	13:38:56	48.19	11.79	6.6	1.5	1.61	2
7		20-Dec-2016	03:30:51	48.19	11.79	3.0	1.8	1.83	7
8		09-Sep-2017	17:20:29	48.19	11.79	3.0	2.1	2.05	8

Table 3 Parameter ranges of the recorded earthquakes in Insheim, described in previous studies (Taddei et al. 2022). Not all 20 selected stations recorded all 13 events.

Number of events	**Date** (dd-mm-yyyy)		**LON** (°)	**LAT** (°)	**Depth** (km)	M_L	M_w	**Recording stations**
13	18-Oct-2009	14-Jul-2016	[49.141, 49.162]	[8.146, 8.164]	[3, 6]	[1.5, 2.2]	[1.6, 2.05]	20 (E,N,V each)

4 Data elaboration

The focus of the research task lies on the effects of the induced seismicity on the building vibrations; therefore, the primary ground motion parameters are the peak ground acceleration (PGA), the peak ground velocity (PGV), considering all channels and distances, and the acceleration response spectra the for the vertical component (SAV) and the geometric mean of the two horizontal components (SAH). We also included the vertical (SVV) and the horizontal (SVH) velocity response spectra. The range of the considered natural periods spans between 0.01 s to 1 s, corresponding to a natural frequency range of 1-100 Hz. We included very short periods to investigate the corresponding input frequency content, which gives insight into a possible activation of the bending modes of walls and ceilings, usually detected between 10 and 40 Hz. A standard damping ratio of 5% was applied.

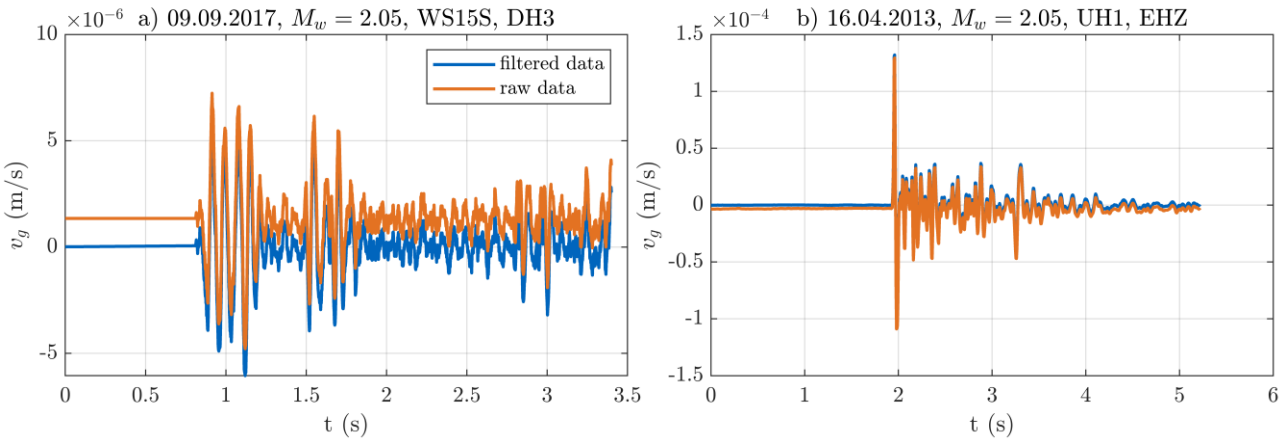

Figure 3. Demonstration of waveform enhancement using baseline correction and bandpass filters. The details about the events, stations, and channels are given above each subplot.

Traditionally, spectral quantities have commonly been approximated as pseudo-spectral quantities, which are calculated from the spectral displacement of a single-degree-of-freedom (SDOF) system assuming harmonic oscillations. This is a significant approximation as seismic signals are not harmonic but highly transient. For accelerations, it can be demonstrated that, at short natural periods (acceleration-sensitive range), this approximation is acceptable. Therefore, the comparison between ground motion data and GMPE predictions is performed using the horizontal pseudo spectral accelerations ($PSAH$). However, concerning the velocities at short natural periods, relying on the pseudo-velocity approximation can result in significant overestimation errors (Samdaria et al. 2018). Therefore, no approximation is adopted for the velocities.

Figure 4 shows the distributions of the considered $\mathrm{M_w}$, epicentral distances r_{epi} and hypocentral distances r_{hyp} for the different locations. From the pool of recorded and simulated data, we restricted further evaluations for $0 \leq \mathrm{r_{epi}} \leq 4$ km and $3 \leq r_{hyp} \leq 11$ km. Figure 5 shows the PGV and the PGA for all events, all stations, and all channels, as a function of the r_{epi}. Usually, GMPEs assume that the logarithm of the spectral quantity decays with the logarithm of r_{epi}. However, one can see that at very short distances this trend cannot be applied. As observed in (Keil et al. 2022), the scattered plots show that the peak ground acceleration (as well as velocity) remains relatively constant or experiences a slight increase with distance up to ca. $r_{epi} = 2.5$ km. Beyond this point, it decreases rapidly for larger distances. For the event with the largest $\mathrm{M_w} = 2.8$, which is simulated and hypothetical, the PGV reaches values > 10 mm/s, which would greatly exceed the limit (5 mm/s) to exclude possible cosmetic damage to normal residential buildings according to the German standard (DIN 4150-3:2016-12).

Table 4 Summary of the input parameters for the simulations of the Munich scenarios.

Input Parameter	**Values used for simulations**
Epicenters coordinates (GK 31468, m)	X = [4466110, 4472884]; Y = [5330852, 5332327]
Source model	Single point source with a delta-pulse time function
Seismic Momen, $M_0 = \frac{1}{10^7} 10^{1.5(M_w+10.7)}$ (Nm)	[6.3096e+09, 1.7783e+13]
Stress drop parameter, $\Delta\sigma$ (bars)	[20, 50]
Attenuation, κ	~0.04
Density, ρ (kg/m^3)	Varies between 2300 and 2900
S-wave velocity, β (m/s)	Increases from 350 to 3526 over 5 km depth
P-wave velocity, α (m/s)	Increases from 1050 to 6100 over 5 km depth
M_w	[0.5, 2.8]
Depth (km)	[3.02, 4.0]
Strike (°)	[55, 75]
Dip (°)	[78, 80]
Rake (°)	-15

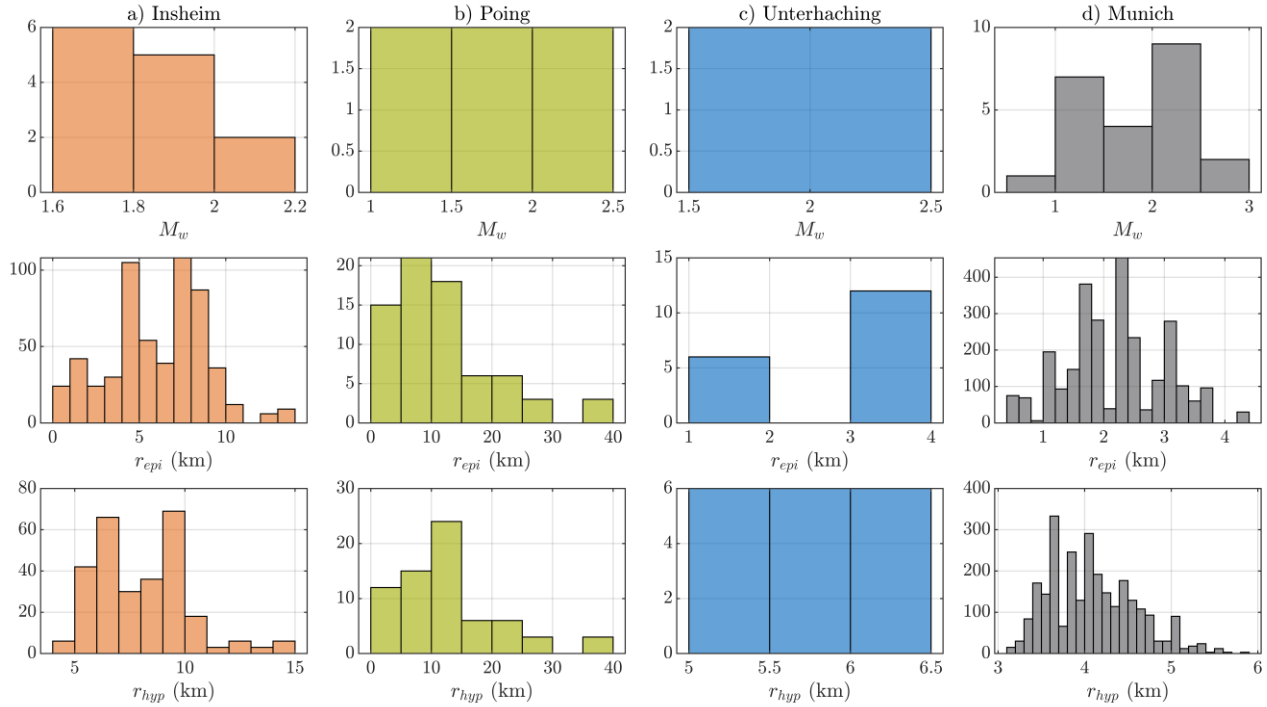

Figure 4. Distributions of M_w, epicentral distances r_{epi} and hypocentral distances r_{hyp} for all signals and locations. The description of the Insheim data is presented in a previous study (Taddei et al. 2022).

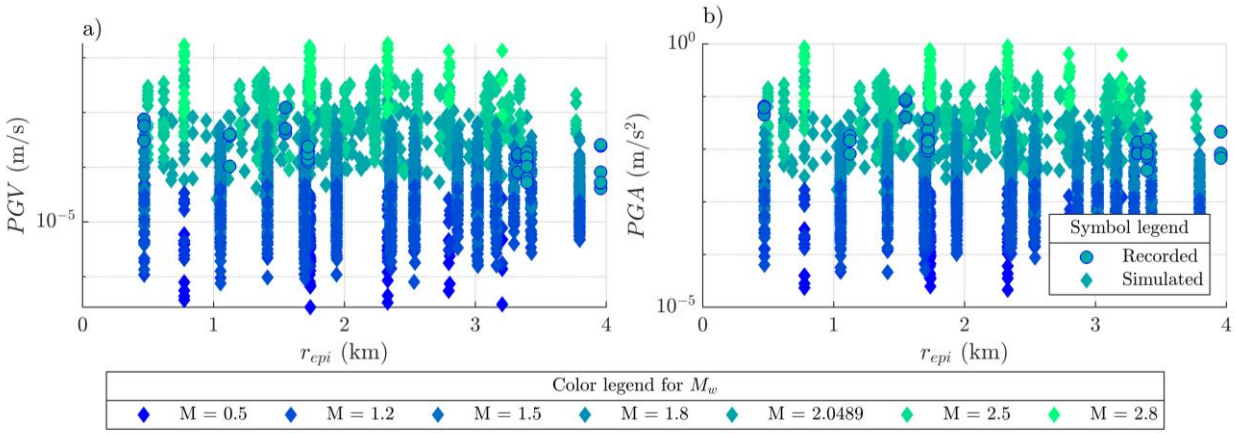

Figure 5. a) PGV and b) PGA for all locations, events, stations, and channels as a function of the r_{epi}.

When dealing with structural vibrations, it is important to investigate the spectral quantities and not only the absolute maximum value.

Figure 6 and Figure 7 show the horizontal and vertical spectral velocities, SVH and SVV, respectively, as a function of the period and for different bins of $\mathrm{M_w}$ and r_{hyp}. The magnitude range is limited to the recorded values, $1.5 \leq \mathrm{M_w} \leq 2.1$. Different colours are assigned to different locations; continuous lines indicate the mean curve for each location and bin, while dotted lines indicate the single samples in each bin. The 4 numbers in each subplot indicate the number of samples for each bin and for each location, according to the relative colour. This representation is adopted for all the trellis plots in the following paragraphs.

In general, the station-to-station variability (max. distance between samples) for a single location within one bin can be of the order of 10. In cases where there are multiple samples for various locations within a bin, it can be deduced that the variability arising from site effects falls within the range of station-to-station variability for a single location. The simulation data aligns with the variability seen in the recorded data, particularly for periods exceeding 0.1 s. Notably, for SVV, the highest values are observed between 0.05 s and 0.1 s, indicating

significant input spectral content between 10 and 20 Hz. In contrast, SVH shows maxima above 0.1 s. Therefore, it's evident that the simulated data cannot be employed for calibrating GMPEs for vertical oscillations due to the imposed 10 Hz cutoff frequency.

5 GMPE model

For this contribution, we reviewed several GMPE models for GI-seismicity and we selected the one proposed by (Douglas et al. 2013). They introduced a comprehensive set of 36 ground motion models for GI-events, considering various parameters like Q (200, 600, and 1800) and κ (0.005, 0.02, 0.04, and 0.06 s) for the attenuation and $\Delta\sigma$ (1, 10, and 100 bar) for the stress-drop. These models aim to encompass the observed variability in median ground motions for induced seismicity. An important aspect is the high variability in predictions from the derived stochastic models at very short periods, especially relevant for addressing building serviceability and comfort issues. This variability is included in the 36 empirical models as aleatory variability rather than treating it as epistemic uncertainty. The practical applicability of the developed stochastic model for hazard assessments is made possible by fitting the predicted quantities for the different scenarios, magnitudes and distances into the functional form in Eq. (2) by regression analysis. The corresponding coefficients and relative standard deviations are provided in the form of a table in (Douglas et al. 2013).

$$\ln Y = b_1 + b_2(M_w - 3) + b_3(M_w - 3)^2 + b_4(M_w - 3)^3 + b_5 \ln(r_{hyp} + b_h) + b_6\,(r_{hyp} + b_h) \qquad (2)$$

Among the 36 available models, the most appropriate one can be chosen using a logic tree process. Subsequently, weights can be assigned to these selected models, considering the availability of seismograms throughout the project's development. This adaptive reassessment permits the fine-tuning of model selection using observed data, ensuring a precise depiction of ground motions at the site and effectively addressing the challenges associated with choosing suitable models for induced seismicity.

For $0.4 < M_w < 2.1$, it can be demonstrated that the stress-drop parameter has limited influence. Therefore, we set $\Delta\sigma = 10$ bar. Most of the records are from narrow distances, and consequently, it was not possible to determine Q, which was assumed to be equal to 1800 (low attenuation). Therefore, we reduced the 36 potential GMPEs to four models, specifically those with κ values of 0.005, 0.02, 0.04, and 0.06 s.

6 Comparison between data and GMPE

Section 4 illustrated the substantial inherent variability in observed ground motion data from small earthquakes. Choosing a single preferred model over others poses challenges due to this variability. Figure 8 shows the comparison between observations, simulations and GMPE predictions, in terms of $PSAH$. There is a significant discrepancy between observations and predictions, especially at short periods. However, the models for $\kappa = 0.02$ and $\kappa = 0.04$ might be appropriate, for the subsequent steps of weighting and averaging, including the relative deviation. The standard deviations of the GMPEs were not considered in this study and will be the object of future research activities. This is necessary due to the high epistemic uncertainty when conducting seismic hazard assessments based on limited observations, as in this study.

7 Conclusion and outlook

This contribution delves into the comprehensive characterization of ground motions resulting from GPP-induced micro-earthquakes in Southern Germany. The focus lies on spectral quantities. We conducted a statistical analysis of available seismic datasets within the Greater Munich Area. Integrating this limited dataset with physics-based simulations, we created a hybrid dataset for comparison with an established GMPE model.

The comparison between recorded and simulated data reveals critical insights. Notably, the imposed cutoff frequency of 10 Hz in the simulations can introduce significant errors, particularly in the amplitudes of the vertical spectral velocities. Moreover, a significant degree of variability for all the data at shorter periods becomes clear.

Our study also highlights disparities between the data and the selected GMPEs for GI-earthquakes, particularly at short periods. One likely factor contributing to this mismatch is the estimation of moment magnitude for small earthquakes. Future research endeavors will explore alternative scaling expressions for computing moment magnitude from local magnitude, including the corresponding standard deviation, and will explore novel regression techniques to better align the data with alternative backbone curves for spectral velocities.

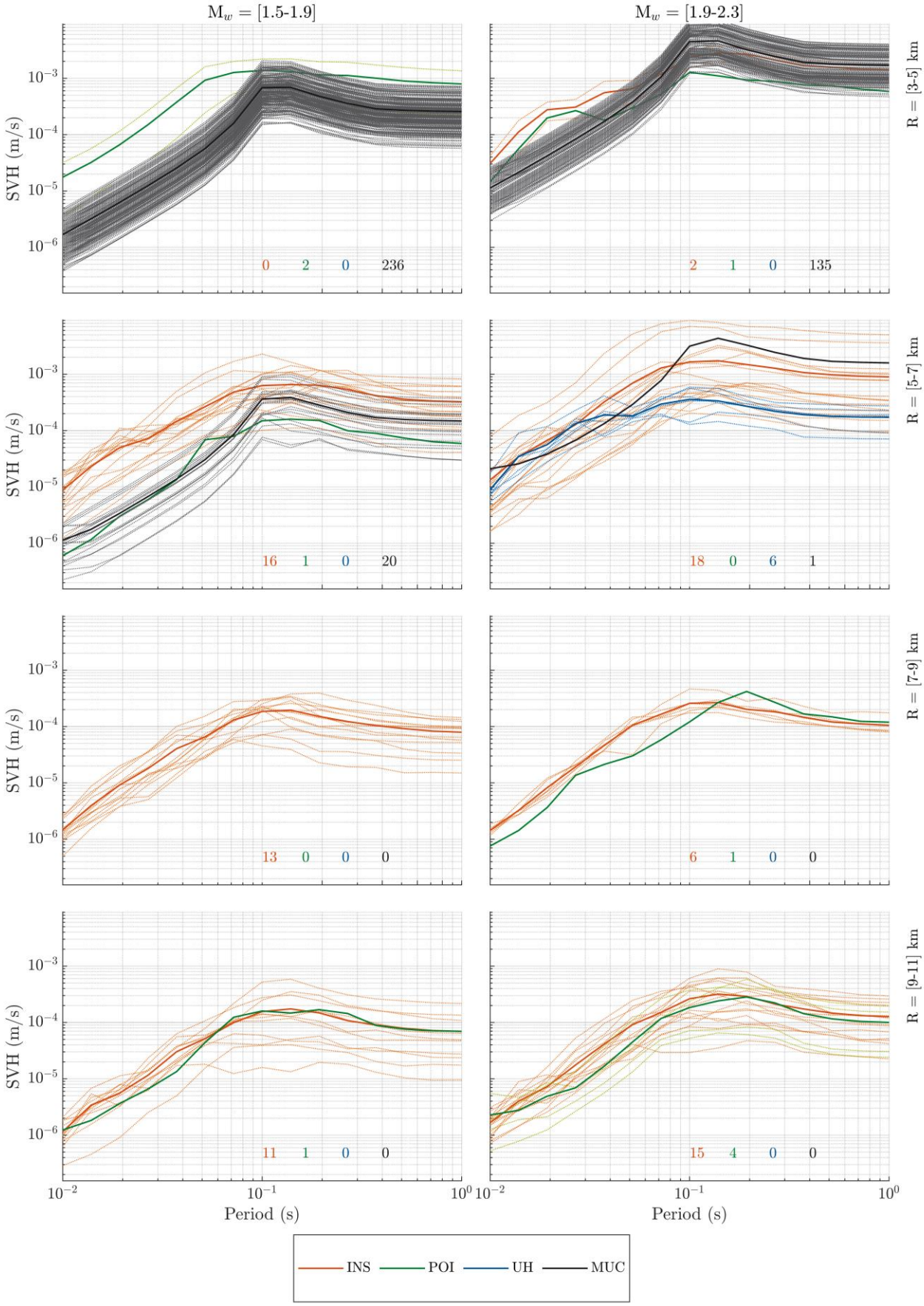

Figure 6 Trellis plots comparing the observed SVH at different locations. See the description in the text.

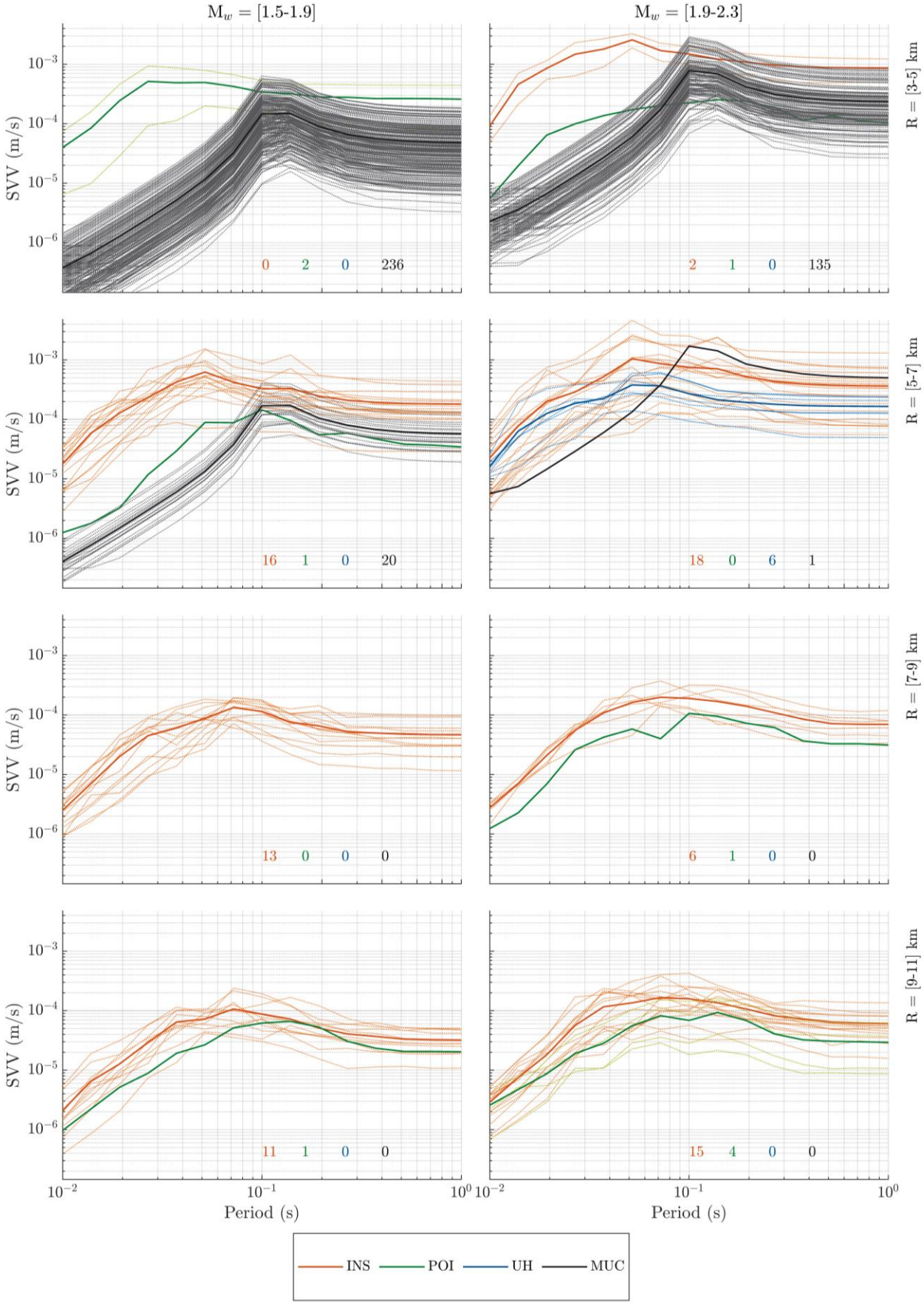

Figure 7 Trellis plots comparing the observed SVV at different locations. See the description in the text.

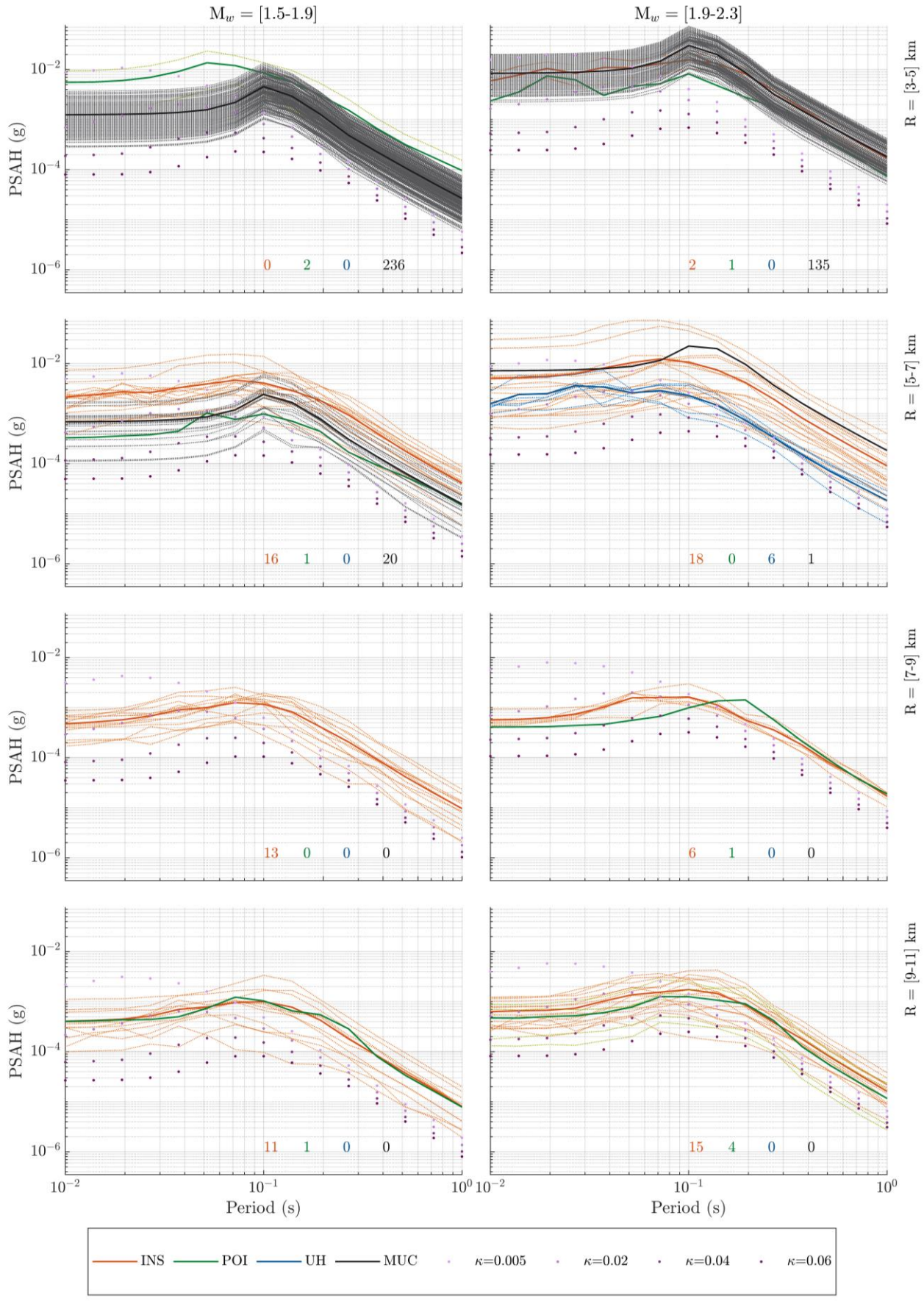

Figure 8 Trellis plots comparing the $PSAH$ for the observations, simulations, and predictions from the GMPEs (for $Q = 1800$, $\Delta\sigma = 10$ bar and varying κ). See the description in the text.

8 Acknowledgements

The authors thank the Bavarian State Ministry for Science and Art (Bayerisches Staatsministerium für Wissenschaft und Kunst) for funding this research within the collaborative research project Geothermie Allianz Bayern (GAB). Sincere gratitude goes to Prof. Julian J Bommer for his invaluable insights and guidance.

9 References

Afanasiev, Michael, Christian Boehm, Martin van Driel, Lion Krischer, Max Rietmann, Dave A May, Matthew G Knepley, and Andreas Fichtner. 2019. “Modular and Flexible Spectral-Element Waveform Modelling in Two and Three Dimensions.” *Geophysical Journal International* 216 (3): 1675–92.

Baker, Jack W, and Abhineet Gupta. 2016. “Bayesian Treatment of Induced Seismicity in Probabilistic Seismic-Hazard Analysis.” *Bulletin of the Seismological Society of America* 106 (3): 860–70.

Beichel, K, R Koch, and M Wolfgramm. 2014. “Die Analyse von Spülproben Zur Lokalisierung von Zuflusszonen in Geothermiebohrungen. Beispiel Der Bohrungen Gt Unterhaching 1/1a Und 2.(Süddeutschland, Molassebecken, Malm).” *Geologische Blätter Für Nordost-Bayern.* 64 (1--4): 43–65.

Bommer, Julian J, Bernard Dost, Benjamin Edwards, Peter J Stafford, Jan van Elk, Dirk Doornhof, and Michail Ntinalexis. 2016. “Developing an Application-Specific Ground-Motion Model for Induced Seismicity.” *Bulletin of the Seismological Society of America* 106 (1): 158–73.

DIN 4150. 2016-12. “DIN 4150-3: Structural Vibrations--Part 3: Effects on Structures.” German Standards Organization (GSO) Berlin.

Douglas, John, Benjamin Edwards, Vincenzo Convertito, Nitin Sharma, Anna Tramelli, Dirk Kraaijpoel, Banu Mena Cabrera, Nils Maercklin, and Claudia Troise. 2013. “Predicting Ground Motion from Induced Earthquakes in Geothermal Areas.” *Bulletin of the Seismological Society of America* 103 (3): 1875–97.

Edwards, Benjamin, Bettina Allmann, Donat Fäh, and John Clinton. 2010. “Automatic Computation of Moment Magnitudes for Small Earthquakes and the Scaling of Local to Moment Magnitude.” *Geophysical Journal International* 183 (1): 407–20.

Edwards, Benjamin, and John Douglas. 2013. “Selecting Ground-Motion Models Developed for Induced Seismicity in Geothermal Areas.” *Geophysical Journal International* 195 (2): 1314–22.

Grünthal, Gottfried. 2014. “Induced Seismicity Related to Geothermal Projects versus Natural Tectonic Earthquakes and Other Types of Induced Seismic Events in Central Europe.” *Geothermics* 52: 22–35.

Grünthal, Gottfried, Dietrich Stromeyer, and Rutger Wahlström. 2009. “Harmonization Check of M w within the Central, Northern, and Northwestern European Earthquake Catalogue (CENEC).” *Journal of Seismology* 13: 613–32.

Keil, Sabrina, Joachim Wassermann, and Tobias Megies. 2022. “Estimation of Ground Motion Due to Induced Seismicity at a Geothermal Power Plant near Munich, Germany, Using Numerical Simulations.” *Geothermics* 106: 102577.

Khansefid, Ali, Ali Bakhshi, and Anooshiravan Ansari. 2019. “Development of Declustered Processed Earthquake Accelerogram Database for the Iranian Plateau: Including near-Field Record Categorization.” *Journal of Seismology* 23 (4): 869–88.

Khansefid, Ali, Seyed Mahmoudreza Yadollahi, Gerhard Müller, and Francesca Taddei. 2022. “Ground Motion Models for the Induced Earthquakes by the Geothermal Power Plants Activity.” *Journal of Earthquake Engineering*, 1–30.

Samdaria, Nikhil, and Vinay K. Gupta. 2018. “A New Model for Spectral Velocity Ordinates at Long Periods.” *Earthquake Engineering and Structural Dynamics* 47 (1): 169–94. https://doi.org/10.1002/eqe.2945.

Sisi, Aida, J Schlittenhardt, and Thomas Spies. 2017. “Probabilistic Seismic Hazard Analysis Of Induced Seismicity In Southern Germany.” In *15. Earthquake Engineering and Structural Dynamic, Weimar, Germany*.

Steinberg, Andreas, Manuel Hobiger, Peter Gaebler, Hannes Vasurya-Bathke, and Aida Azari Sisi. 2023. “Framework for Deterministic Earthquake Ground Motion Maps in Germany Using Machine Learning.” In *XXVIII General Assembly of the International Union of Geodesy and Geophysics (IUGG)*.

Taddei, F, A Kumawat, A Csuka, R Cudmani, and G Müller. 2022. “Input Characterisation for Low-Amplitude Seismicity Induced by Geothermal Operations.” In *International Conference on Noise and Vibration Engineering (ISMA)*.

Wolfgramm, Markus, Jörn Bartels, F Hoffmann, G Kittl, G Lenz, P Seibt, R Schulz, R Thomas, and H J

Unger. 2007. “Unterhaching Geothermal Well Doublet: Structural and Hydrodynamic Reservoir Characteristic; Bavaria (Germany).” In *European Geothermal Congress*. Vol. 30.

Annex

Table 5. Stations-events matrix for Poing and Unterhaching.

	Poing						Unterhaching	
Station list	19-Nov-2016 17:41:05	27-Nov-2016 14:52:21	07-Dec-2016 05:28:54	10-Dec-2016 13:38:56	20-Dec-2016 03:30:51	09-Sep-2017 17:20:29	16-Apr-2013 21:51:42	16-Apr-2013 21:51:48
BHF1S					x			
HIS8S			x					
HWMRS						x		
LP01S	x	x	x		x	x		
MS1						x		
POI01					x			
POI02					x			
POI03					x			
Poing					x	x		
RHS26						x		
SCH6S						x		
SIS21			x			x		
WS15S	x		x	x	x	x		
UH1							x	x
UH2							x	x
UH3							x	x

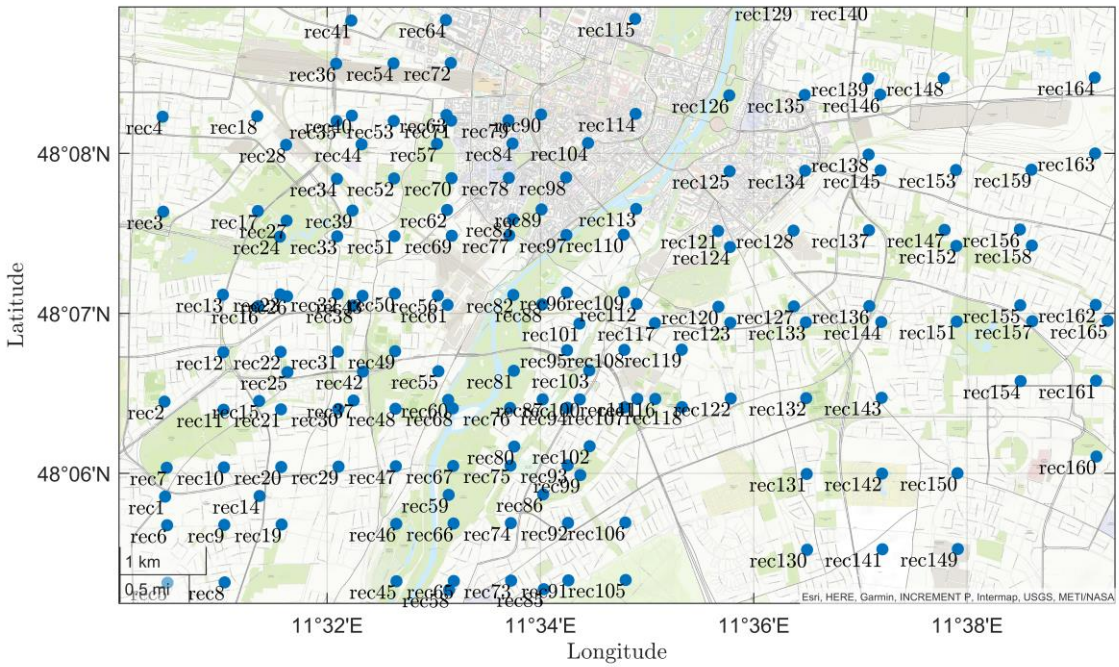

Figure 9 Distribution of stations for the simulations of the Munich scenarios. Not all the stations recorded all the 23 events.